Vibrational and quasiharmonic thermal properties of CaO under pressure

Bijaya B. Karki[1] and Renata M. Wentzcovitch[2]

[1]*Department of Computer Science, Louisiana State University, Baton Rouge, Louisiana 70803, USA*
[2]*Department of Chemical Engineering and Materials Science and Minnesota Supercomputing Institute, University of Minnesota,*
Minneapolis, Minnesota 55455, USA
(Received 23 July 2003; published 11 December 2003)

We have investigated by first principles the phonon dispersions of CaO across its pressure induced phase transformation from the B1 (NaCl structure) to the B2 (CsCl structure) phase. Beyond their stability fields we have uncovered phonon instabilities that should be associated with this phase transition. We have also used these dispersions in conjunction with the quasiharmonic approximation (QHA) to calculate several thermodynamic properties in both phases. Comparisons between the predicted properties with experimental measurements and with similar properties of MgO indicate that the QHA is quite unsatisfactory for CaO. Despite this, the calculated transition pressure at room temperature falls within the range of measurements. This transition is shown to have a negative Clapeyron slope.

I. INTRODUCTION

The behavior of lattice vibrations under pressure provides useful information regarding structural instabilities and phase transformations. It can also be used to derive thermodynamic properties within the quasiharmonic approximation (QHA). While this approach to thermodynamics may be valid up to temperatures between the Debye temperature θ_D and the melting temperature T_M for stable crystals,[1,2] it may fail even below θ_D in the presence of soft modes. CaO is a simple but interesting case because it transforms from the B1 (NaCl structure) to the B2 phase (CsCl structure) at pressures in the range of 50–70 GPa[3–5] and has lattice instabilities in this pressure range. Perhaps, more importantly, the thermodynamics of the related mineral periclase, MgO, has been extensively studied using this approach and the QHA has been shown to be very successful in this case. Comparison between the predicted thermodynamic properties of both solids establishes a clear case against the use of the QHA for CaO. While the static structural and elastic properties of CaO have previously been studied at high pressure by first principles,[6,7] its phonon spectrum has so far been studied only at zero pressure.[8] Neutron-scattering data are also limited to low pressure.[9–11] Here we report phonon dispersions for CaO in the B1 and B2 phases, examine the validity of QHA, and explore the B1-B2 phase boundary.

II. METHODOLOGY

Computations are performed using the local-density approximation (LDA)[13] and Troullier-Martins pseudopotentials.[14] The Ca pseudopotential is generated from $3s^2 3p^4 3d^0$ (p locality, $r=2.0$ a.u) whereas the O pseudopotential is generated from $2s^2 2p^4$ (p locality, $r=1.45$ a.u.). A plane-wave basis set with cutoff energy of 90 Ry is used to expand electronic wave functions. Brillouin-zone summations are performed over six and four special k points for the B1 and B2 phases, respectively.[15]

The dynamical matrix elements were calculated on a 4 ×4×4 q grid by performing linear-response calculations us-

ing density-functional perturbation theory.[12] They are then interpolated at various **q**'s to offer bulk phonon dispersions. The LO-TO splitting at Γ is obtained from the nonanalytical contribution of the macroscopic electric field to the force constant tensor expressed in terms of Born effective charges **Z***) and dielectric constant (ϵ_∞) which are also calculated self-consistently.

III. RESULTS AND DISCUSSION

A. Lattice dynamics

In the B1 and B2 phases atoms are sixfold and eightfold coordinated, respectively. The nearest-neighbor distances correlate with coordination numbers while vibrational frequencies anticorrelate with nearest-neighbor distances. The vibrational band widths of these phases at the same pressure can therefore be understood in terms of this coordination change. This trend in frequencies has predictable effects on some thermodynamic properties of a quasiharmonic solid. These effects will be explored closely in the following section.

Figures 1(a) and 1(b) show bulk phonon dispersions of CaO at low and high pressures in the B1 and B2 phases. Neutron-scattering data[9–11] and results from a previous calculation[8] at zero pressure for the B1 phase are reproduced within a few percent [see Fig. 1(a) and Table I]. These results show that the vibrational spectra of CaO in both phases depend strongly on pressure. Most mode frequencies increase monotonically with pressure at various rates but a few phonons in the B1 phase soften with compression. In particular, instabilities develop in the lowest acoustic branches around the X point of the Brillouin Zone (BZ) at pressures above 120 GPa. The overall frequency increase with pressure is reflected in significant changes in the vibrational density of states (VDoS) [Figs. 1(a) and 1(b)] with major peaks fading with pressure.

Under decompression the B2 phase's VDoS develops a peak at intermediate frequencies while the high-frequency peak weakens. A peculiarity of this dispersion is the position of a maximum between Γ and X. Under decompression all frequencies decrease but the lowest acoustic branch becomes
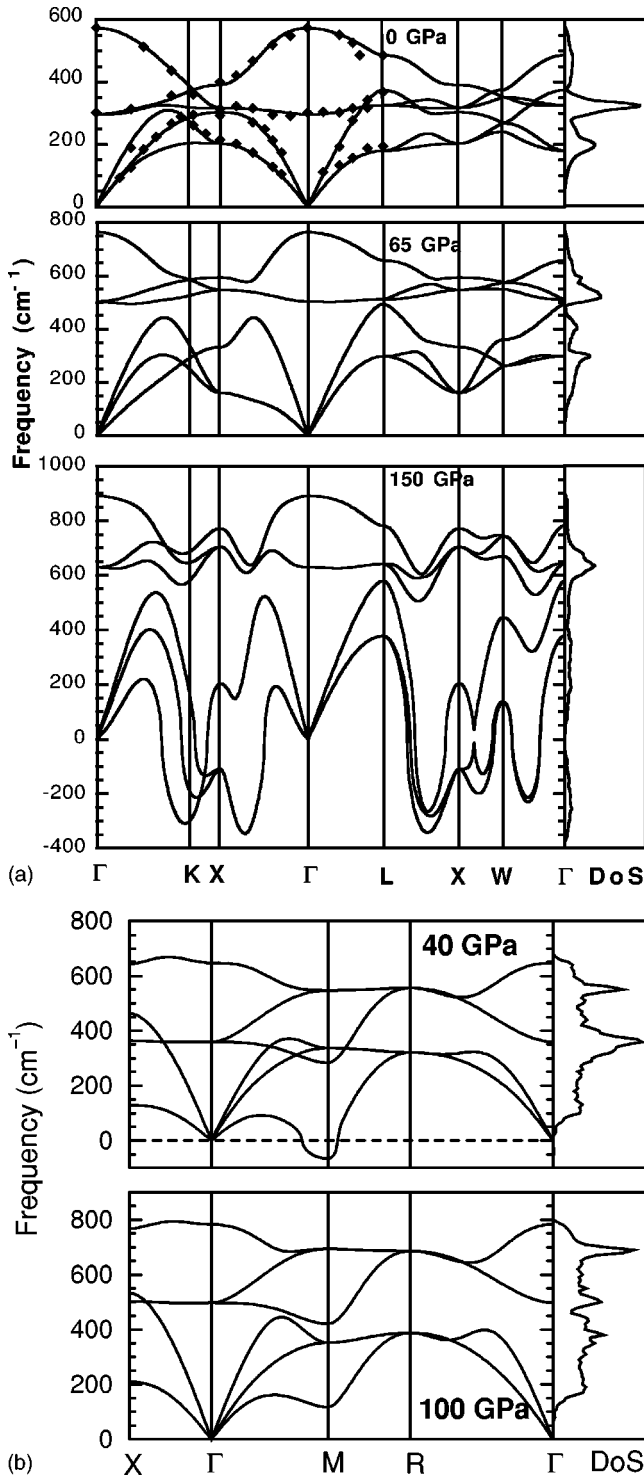
FIG. 1. Phonon dispersions of (a) B1 phase at 0, 65, and 150 GPa; (b) B2 phase at 40 and 100 GPa. Symbols are experimental data at ambient condition.[9–11]

unstable around the M point of the BZ around 50 GPa. Our calculated static transition pressure is 55 GPa [see Sec. III C]. Therefore, the identified instabilities in both phases, that should be associated with the B1-B2 phase change, develop outside their stability fields, much more so for the B1 than for the B2 phase.

Figure 2 shows the calculated volume dependence of high-symmetry phonon frequencies and the LO-TO splittings. Most LO-TO splittings vary little with pressure, suggesting a weak pressure dependence of Born-effective charges and dielectric constant (Fig. 3). Their zero pressure values for the B1 phase are $\mathbf{Z}^*(\text{Ca}) = 2.396$, $\mathbf{Z}^*(\text{O}) = -2.334$, $\epsilon_\infty = 3.828$, compared to the experimental[16] charge of 2.073 and dielectric constant of 3.27. The LO-TO splittings at Γ, X, and L in the B1 phase are in excellent agreement with the experimental data (Table I). Only at high-symmetry points where the lattice instabilities develop under pressure these splittings seem to vary rapidly. In the B1 phase this happens at the X-point. The splitting between the unstable X_{TA} and X_{LA} mode frequencies also varies rapidly with pressure.

Something similar happens in the B2 phase: anomalous behavior takes place at the high-symmetry point around which the instability develops. The M_{LA} mode frequency rapidly decreases with decompression and eventually becomes unstable while the M_{TA} mode shows a weak linear volume dependence. Another anomaly at the M point is the negative LO-TO splitting, i.e., $\omega_{M_{\text{TO}}} > \omega_{M_{\text{LO}}}$.

B. Thermodynamic properties

We have used these volume dependent VDoS's to investigate thermodynamic properties using the QHA for the Helmholtz free energy.[1] This is

$$F(V,T) = E_0(V) + \frac{1}{2} \sum_{\mathbf{q},j} \hbar \omega_j(\mathbf{q},V)$$

$$+ k_B T \sum_{\mathbf{q},j} \ln\{1 - \exp[-h\omega_j(\mathbf{q},V)/k_B T]\}. \quad (1)$$

The first term is the internal energy obtained from static discrete fourier transform calculations. The second and third are contributions from the zero-point motion and from thermal excitations, respectively. The summation over modes is performed on a $12 \times 12 \times 12$ regular $\mathbf{q}$ mesh. Comparison with results derived from an $8 \times 8 \times 8$ mesh indicates that the thermodynamic properties reported here should be converged to better than 0.1%. The first step in the calculations is to fit $F(V,T)$ to a fourth-order finite strain expansion[17] at each T. Thermal properties are then derived from these isothermal equations of state using standard thermodynamic relations. Several of these properties in both phases are compared with available experimental data and with those of MgO in Table II.

Volume-pressure isotherms for both phases are displayed in Fig. 4. The 300 K isotherm lies systematically below the experimental one.[3–5] The calculated lattice constant at ambient conditions is 1.7% smaller than the measured value while the bulk modulus is ~7% larger (see Table II). Our static equations of state (EoS) for both phases are represented by the dashed lines. The static EoS parameters for the B1 phase are $a_0 = 4.703$ Å, $K_0 = 130$ GPa, and $K'_0 = 4.37$, in close agreement with previous all-electron LDA-LAPW results of 4.714 Å, 129 GPa, and 4.47, respectively.[7] The contributions of zero-point motion and thermal energies to the 300 K EoS are not sufficient to remove the discrepancy with respect to

TABLE I. Calculated zero pressure phonon frequencies (in cm^{-1}) and their volume derivatives (in $cm^{-1}/Å^3$) of CaO at Γ, X, and L compared with experiments (Refs. 9–11), and previous calculations for CaO (Ref. 8) and MgO (Ref. 2).

	Γ_{TO}	Γ_{LO}	X_{TA}	X_{LA}	X_{TO}	X_{LO}	L_{TA}	L_{LA}	L_{TO}	L_{LO}
This study, ω	297	575	203	305	318	392	180	375	326	487
$d\omega/dV$	4.3	3.6	0.2	3.9	4.4	1.6	2.3	3.7	2.2	3.2
Expt. ω	302	575	216	294	314	400	195	368		473
Previous calculation, ω	297	570	214	321	320	392	203	388	328	486
MgO, ω	414	710	289	433	464	555	287	548	371	570
MgO, $d\omega/dV$	7.7	6.1	1.5	4.8	7.7	5.8	4.7	5.9	4.2	5.5

room-temperature experimental results (see Table II). This contrasts with the case of MgO, where the typical LDA overbinding reflected in these parameters is removed after inclusion of these contributions.[2]

Before proceeding it is useful to define some quantities and display the quasiharmonic formulas for several thermodynamic quantities and properties. For sake of notation simplification, $(\mathbf{q},j) \rightarrow i$, and $(\hbar \omega_i/k_B T) = x_i$. The entropy, internal energy, and specific heats at constant volume and pressure are

$$S(V,T) = \sum_i S_i(V,T)$$

$$= k_B \sum_i \left[-\ln(1 - e^{-x_i}) + k_B \frac{x_i}{(e^{x_i} - 1)} \right], \quad (2)$$

$$E(V,T) = E(V,0) + E^{TH}(V,T), \quad (3)$$

where

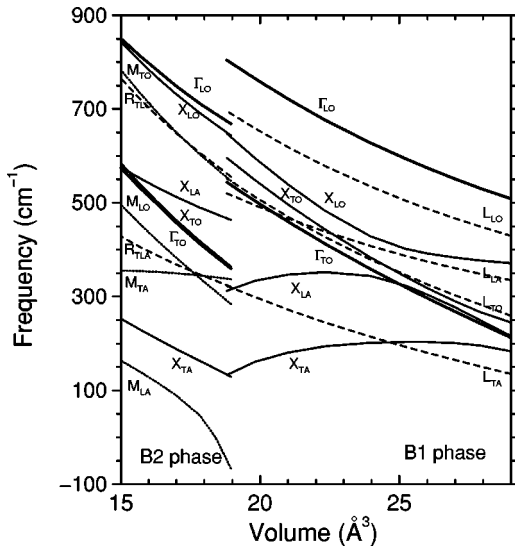$$E^{TH}(V,T) = \sum_i E_i^{TH}(V,T) = \sum_i k_B T \frac{x_i}{[e^{x_i} - 1]}, \quad (4)$$

$$C_V(V,T) = \sum_i C_{Vi}(V,T) = k_B \sum_i e^{x_i} \left(\frac{E_i^{TH}}{k_B T} \right)^2, \quad (5)$$

$$C_P = C_V(1 + \alpha \gamma T), \quad (6)$$

where γ is the thermal Grüneisen parameter

$$\gamma(V,T) = \frac{\sum_i \gamma_i C_{Vi}}{C_V} \quad (7)$$

with

$$\gamma_i = -\frac{\partial \ln \omega_i}{\partial \ln V}. \quad (8)$$

The thermal-expansion coefficient can be expressed as

$$\alpha = \frac{1}{K_T} \frac{\partial P^{TH}}{\partial T}, \quad (9)$$

where P^{TH} the thermal pressure, and K_T the isothermal bulk modulus are given by

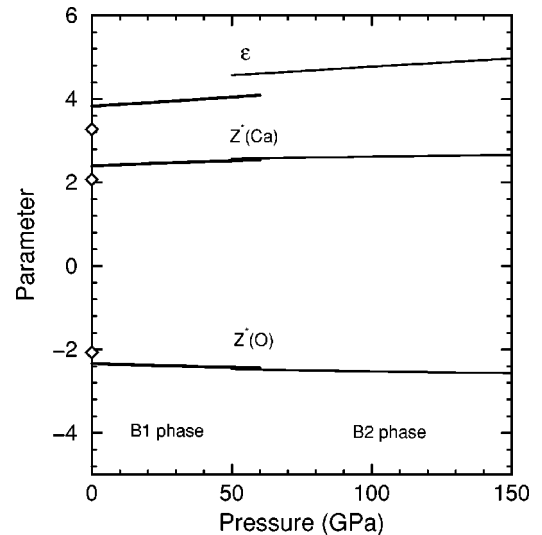FIG. 2. Volume dependence of the frequencies of high-symmetry phonons.

FIG. 3. Pressure dependence of Born-effective charges and dielectric constant. Experimental data are indicated by symbols (Ref. 16).

TABLE II. Thermodynamical parameters of CaO calculated within the QHA compared with experiments (Refs. 18,19).

	300 K Calculated	300 K Expt.	300 K Calculated [a]	300 K Expt. [a]	1000 K Calculated	2000 K Calculated
			B1 phase at 0 GPa			
a (Å)	4.727	4.81	4.22	4.21	4.777	4.896
K_T (GPa)	121	111, 115	159	160	98	55
$\partial K_T/\partial P$	4.58	4.1, 4.8	4.30	4.15	5.27	7.70
$\partial^2 K_T/\partial P^2$ (GPa^{-1})	-0.048		-0.030		-0.10	-0.55
$\partial K_T/\partial T$ (GPaK^{-1})	-0.029	-0.021	-0.027	-0.027	-0.036	-0.056
$\alpha \times 10^{-1}$ (K^{-1})	3.56	3.04	3.10	3.12	5.35	10.86
γ_{th}	1.64	1.35	1.54	1.54	1.75	2.12
C_P (J mol^{-1}K^{-1})	42.54	30.52	37.06	37.67	53.76	73.36
S (J mol^{-1}K^{-1})	40.01		26.65		98.98	140.32
			B1 phase at 60 GPa			
a (Å)	4.320		3.91		4.330	4.347
K_T (GPa)	356		387		342	321
$\alpha \times 10^{-1}$ (K^{-1})	0.67		0.97		1.10	1.23
γ_{th}	0.83		1.17		0.95	0.99
C_P (J mol^{-1}K^{-1})	35.2		29.02		48.7	50.7
S (J mol^{-1}K^{-1})	27.3		16.9		80.2	114.7
			B2 phase at 60 GPa			
a (Å)	2.621				2.633	2.656
K_T (GPa)	360				335	297
$\alpha \times 10^{-1}$ (K^{-1})	1.63				2.28	2.69
γ_{th}	1.76				1.73	1.82
C_P (J mol^{-1}K^{-1})	36.4				50.3	54.6
S (J mol^{-1}K^{-1})	30.0				84.4	120.6

[a]Results for MgO are also shown for comparison. Calculations from Ref. 2 and experiments from Ref. 20.

$$\frac{\partial P^{TH}}{\partial T} = \sum_i \frac{\partial P_i^{TH}}{\partial T} = \sum_i \frac{\gamma_i}{V} \frac{\partial E_i^{TH}}{\partial T} = \frac{\gamma C_V}{V}, \quad (10)$$

$$K_T = K_T(V,0) + K_T^{TH} \quad (11)$$

with

$$K_T^{TH} = \sum_i K_{Ti}^{TH} = \sum_i P_i^{TH}\left[2 - q_i - \frac{x_i}{(1-e^{-x_i})}\right], \quad (12)$$

where

$$q_i = \frac{\partial \ln \gamma_i}{\partial \ln V}. \quad (13)$$

The behavior of the *calculated* properties can be interpreted by invoking these expressions and recalling that in the QHA ω_i's do not depend on temperature explicitly but only implicitly through volumetric effects. Regardless of the origin of the change in ω_i's, i.e., structural, chemical, or volumetric changes, S and C_V always increase with decreasing range of $x_i = \hbar\omega_i/k_B T$ or with decreasing center of mass of the VDoS. C_P behaves much like C_V, the difference being about two orders of magnitude smaller. Since K_T is in general larger than P^{TH}, α depends primarily on K_T and secondarily on P^{TH}.

Results in Table II display these trends clearly. Across the B1-B2 phase change ω_i's decrease (see Fig. 1), γ_i's increase (see Fig. 2), V decreases, and K_T's remain similar. According to the quasiharmonic formulas the values of all properties should increase across this phase change and this is indeed displayed by our results at 60 GPa and 300 K. Changes in these properties with increasing temperature, in either phase, can also be rationalized in this way. Comparison between the *calculated* properties of CaO and MgO can also be explained in this way. At 0 GPa the vibrational frequencies and mode Grüneisen parameters of CaO are systematically smaller than those of MgO (see Table I). The larger γ_i's and K_T, and smaller equilibrium volume of MgO in the B1 phase also help to explain the similarity of their thermal expansivities α's at ambient conditions despite the smaller values of CaO's vibrational frequencies (see Table II). The difference between their *calculated* C_P's and S's can also be understood in this way. In summary, the behavior of these properties can be predicted on the basis of these quasiharmonic formulas and knowledge of the overall behavior of the VDoS *"if"* the QHA is valid.

What the QHA expressions cannot explain is the experimental trends of these properties at ambient conditions across these compounds. The volume dependence of α along several isotherms is shown in Fig. 5. The predicted ambient value of 3.56×10^{-5} K^{-1} differs from the experimental
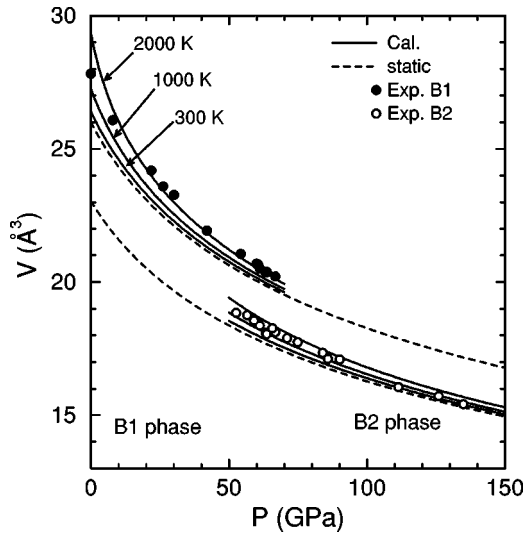
FIG. 4. Pressure-volume equations of state for the static lattice and at 300, 1000, and 2000 K isotherms (lines from bottom to top). Experimental data at room temperature are denoted by symbols (Refs. 3–5).

value of 3.04×10^{-5} K^{-1} for the B1 phase[18] by 17%. This difference increases to more than 35% above 1000 K. These differences are much larger than those of $\sim 0\%$ and 7%, respectively at 300 and 1000 K predicted for MgO (Ref. 2). Similarly, C_P and the thermal Grüneisen parameter γ_{th} of CaO are significantly overestimated (Table II). Presumably S is also overestimated but we did not find experimental values to compare with. While the QHA is shown to work so well for MgO over a wide temperature range,[2] it appears to be inadequate for CaO even at 300 K. Overestimation of α is the fingerprint of the QHA's shortcomings. Even more important is the fact that the experimental values at ambient conditions for the C_P, α, and γ_{th} of CaO are smaller than

MgO's, contrary to quasiharmonic predictions. This implies that the QHA is inadequate even at ambient conditions in the case of CaO.

By no means this inability to reproduce the experimental trends should be attributed to the LDA. If instead we had used the generalized gradient approximation, the volume and bulk modulus of CaO would have increased and decreased, respectively, improving perhaps the agreement between calculated static and experimental ambient condition values. However, with increasing nearest-neighbor distances, there would be an overall decrease in the phonon frequencies. All these changes would contribute to increase the discrepancy between calculated and measured thermodynamic properties.

C. B1-B2 phase boundary

Despite this apparent inadequacy of the QHA for CaO even at ambient conditions where phonons are stable it is worthwhile investigating the B1-B2 phase boundary. This is obtained by comparing the Gibbs free energy of these phases at various pressures and temperatures. The free energies are likely to be incorrect near unstable phonons (120 GPa in the B1, 50 GPa in the B2), but, as we have seen previously (subsection 3.1), this does not occur at the thermodynamical boundary itself.

Our transition pressure is 56 GPa for the static lattice and 54.5 GPa at 300 K, compared to 50–70 GPa from experiments.[3-5] Moreover, the calculated transition pressure decreases with increasing temperature to 47 GPa at 2000 K thus showing a negative Clapeyron slope, dP_T/dT (Fig. 6). This phase boundary may differ somewhat from the correct one because of the inadequacy of the quasiharmonic free-energy expression specially for the B2 phase. However, this phase boundary should indeed have a negative slope since the entropy increases across this phase change ($dP_T/dT = dS/dV$). Not only the entropy increases, but also α, C_P, and γ_{th} increase across the transition (see Table II) despite the volume collapse of about 10% (Fig. 4). These thermodynamic quantities display an abrupt increase across the transition because the vibrational frequencies span a smaller en-
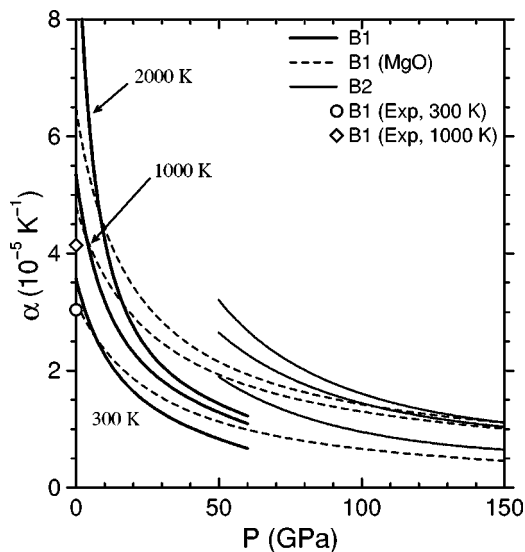

FIG. 5. Thermal expansivity along 300, 1000, and 2000 K isotherms. Experimental data at ambient pressure are from Ref. 18. Previous results on MgO (Ref. 2) are also shown for comparison.
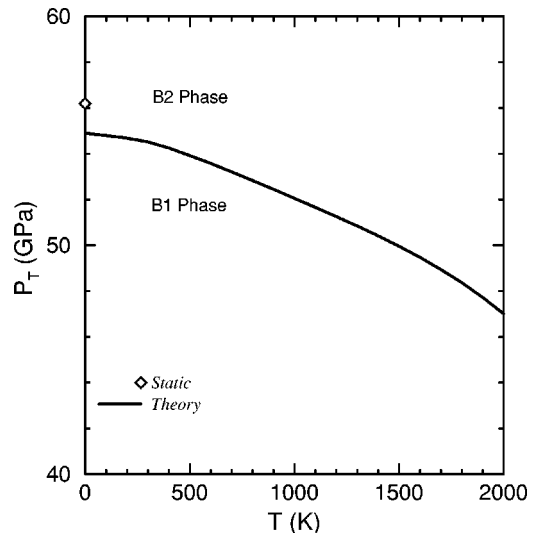

FIG. 6. Calculated B1-B2 phase diagram of CaO.

ergy range in the B2 phase in relation to the B1. As mentioned earlier, this is a consequence of the increase of coordination and nearest neighbor distances across this pressure induced transformation (see Fig. 2. In the absence of instabilities, the smaller the frequency range, the larger the value of these thermodynamic properties.

IV. CONCLUSION

We have investigated and compared the vibrational properties of CaO in the B1 and B2 phases up to 150 GPa. We have identified soft phonon instabilities in both phases that should be associated with the B1-B2 transformation. These occur not at the thermodynamical boundary, but, as expected, outside the stability field of these phases. Comparisons between experimental and calculated specific heats C_P and thermal expansivities, α, of MgO and CaO at ambient con-

ditions, indicate that the QHA is less appropriate for CaO than it is for MgO. These quantities are largely overestimated for CaO and the experimental trends across these solids is not reproduced. CaO, therefore, should be considered an exemplar of inadequacy of the QHA, and a simple system for exploration of more accurate methodologies for free-energy computations. We have also explored the B1-B2 phase boundary and are able to reproduce the experimental transition pressure within the large experimental uncertainty at room temperature. Finally, we have shown that this transition should display a negative Clapeyron slope.

---

[1] D.C. Wallace, *Thermodynamics of Crystals* (Wiley, New York, 1972).

[2] B.B. Karki, R.M. Wentzcovitch, S. de Gironcoli, and S. Baroni, Science **286**, 1705 (1999); Phys. Rev. B **61**, 8793 (2000).

[3] R. Jeanloz, T.J. Ahrens, H.K. Mao, and P.M. Bell, Science **206**, 829 (1979).

[4] J.F. Mammone, H.K. Mao, and P.M. Bell, Geophys. Res. Lett. **8**, 140 (1981).

[5] P. Richet, H.K. Mao, and P.M. Bell Geophys. Res. Lett. **93**, 15 279 (1988).

[6] B.B. Karki and J. Crain, J. Geophys. Res. **103**, 12 405 (1998).

[7] M.J. Mehl, R.E. Cohen, and H. Krakauer, J. Geophys. Res. **93**, 8009 (1988).

[8] O. Schütt, P. Pavone, W. Windl, K. Karch, and D. Strauch, Phys. Rev. B **50**, 3746 (1994).

[9] D.H. Saunderson and G. Peckham, J. Phys. C **4**, 2009 (1971).

[10] P.R. Vijayaraghavan, X. Marsongkohadi, and P.K. Iyengar, in *Proceedings of Symposium on Neutron Inelastic Scattering, Grenoble, France, 1972* (IAEA, Vienna, 1972), p. 95.

[11] K.H. Rieder, B.A. Weinstein, M. Cardona, and H. Bilz, Phys. Rev. B **8**, 4780 (1973).

[12] S. Baroni, P. Giannozzi, and A. Testa, Phys. Rev. Lett. **58**, 1861 (1987).

[13] J.P Perdew and A. Zunger, Phys. Rev. B **23**, 5048 (1981).

[14] N. Troullier and J.L. Martins, Phys. Rev. B **43**, 1993 (1991).

[15] H.J. Monkhurst and J.D. Pack, Phys. Rev. B **13**, 5188 (1976).

[16] M.J.L. Sangster and A.M. Stoneham, Philos. Mag. B **43**, 597 (1981).

[17] F.D. Birch, J. Geophys. Res. **91**, 4949 (1986).

[18] H. Oda, O.L. Anderson, D.G. Isaak, and I. Suzuki, Phys. Chem. Miner. **19**, 96 (1992).

[19] P. Chang and E.K. Grahm, J. Phys. Chem. Solids **38**, 1355 (1977).

[20] D.G. Isaak, O.L. Anderson and T. Goto, Phys. Chem. Miner. **16**, 704 (1989).